Comparative Study of Two Different Hydrogen Redistribution Strategies along a Fluidized-Bed Hydrogen Permselective Membrane Reactor for Methanol Synthesis

M. R. Rahimpour* and M. Bayat

Chemical Engineering Department, School of Chemical and Petroleum Engineering, Shiraz University, Shiraz 71345, Iran

In this work, two different hydrogen redistribution strategies along a bubbling fluidized-bed hydrogen permselective membrane reactor have been compared. In the first strategy, fresh synthesis gas flows in the tube side of the fluidized-bed membrane reactor in cocurrent mode with reacting material in the shell side, so that more hydrogen is provided in the first segments of the reactor. In the second strategy, fresh synthesis gas flows in the tube side of the fluidized-bed membrane reactor in countercurrent mode with reacting material in the shell side, so that more hydrogen is provided in the last segments of the reactor. A dynamic two-phase theory in the bubbling regime of fluidization was developed to model and compare two strategies from different points of view. Comparison between cocurrent and countercurrent modes of operation shows that the reactor in the countercurrent configuration operates with higher conversion of methanol, longer catalyst life, and higher carbon dioxide removal, whereas the reactor in the cocurrent configuration operates with higher carbon monoxide removal, lower water production, and higher hydrogen permeation rate. Enhancement of the carbon dioxide removal in countercurrent mode and the carbon monoxide removal in cocurrent mode causes a lower environmental impact. The lower water production rate in cocurrent mode reduces catalyst recrystallization.

1. Introduction

Methanol is a primary liquid petrochemical that is produced on a large scale in the world as a fuel, solvent, and building block to produce chemical intermediates. It is produced from synthesis gas on a large scale. Synthesis gas consists of carbon dioxide, carbon monoxide, hydrogen, and some inert components such as argon and nitrogen. Rising energy prices and global warming have led to increased interest in alternative fuels. The viability of alcohol as a fuel is a debatable topic, as other energy sources are required for production. Methanol has been considered as a fuel. Because of its physical and chemical characteristics, methanol has proved to be an attractive automotive fuel.[1,2] It has the advantages that it is liquid under normal conditions, it can be stored and transported as easily as gasoline, and it can be used in conventional combustion engines without requiring any major adjustments. Methanol has twice the energy density of liquid hydrogen and can be more conveniently stored and transported.[3,4] Methanol use in current-technology vehicles has some distinct advantages and disadvantages. On the positive side, methanol has a higher octane rating than gasoline. Methanol's high heat of vaporization results in lower peak flame temperatures than gasoline and lower nitrogen oxide emissions. Its greater tolerance to lean-combustion higher air-to-fuel equivalence ratios results in generally lower overall emissions and higher energy efficiency. However, the energy density of methanol is about one-half that of gasoline, reducing the range a vehicle can travel on an equivalent tank of fuel.[5]

1.1. Process and Model. The importance of methanol has motivated numerous studies whose aim was to improve the efficiency of industrial methanol synthesis reactors. A dynamic simulation of a conventional methanol synthesis reactor was performed by Lovik et al. for long-term optimization.[6] Rahimpour et al. studied deactivation of the methanol synthesis catalyst and proposed mechanisms for deactivation of this type of catalyst.[7] Velardi and Barresi proposed a multistage methanol reactor network with autothermal behavior to promote the reactor performance.[8] To improve the performance of methanol reactors, a number of configurations have been proposed, including conventional dual-type reactors,[9,10] fixed bed with hydrogen permselective membrane reactors,[11,12] membrane dual-type reactors,[13−15] fluidized-bed reactors,[16] and fluidized-bed membrane dual-type reactors.[17,18]

The dual-type methanol reactor is an advanced technology for converting natural gas into methanol at low cost and in large quantities. This system is mainly based on a two-stage reactor system consisting of a water-cooled reactor and a gas-cooled reactor. Synthesis gas is fed to the tubes of the gas-cooled reactor (second reactor). This cold feed synthesis gas is routed through tubes of the second reactor in countercurrent flow with the reacting gas and is heated by the heat of the reaction produced in the shell. Therefore, the reacting gas temperature is continuously reduced over the reaction path in the second reactor. The outlet synthesis gas from the second reactor is fed to the tubes of the first reactor (water-cooled), and the chemical reaction is initiated by a catalyst. The heat of reaction is transferred to the cooling water inside the shell of the reactor. In this stage, the synthesis gas is partly converted to methanol in a water-cooled conventional-type reactor. The methanol-containing gas leaving the first reactor is directed into the shell of the second reactor. Finally, the product is removed from the downstream of the second reactor.[19] The operating data for this conventional reactor show a high pressure drop, plug flow, and low performance for gas-cooled reactors in comparison with water-cooled reactors.[19] Also, during operation, catalyst deactivation in gas-cooled reactors is higher than the design values.[19]

1.2. Pd−Ag Membrane. As mentioned above, the reactions in a gas-cooled reactor take place in a large-diameter reactor (shell side) so that radial gradients of concentration and temperature prevent higher performance of this reactor. A membrane reactor combines the chemical reaction and membrane in one system. The application of membrane reaction technology in chemical reaction processes now mainly focuses on reaction systems containing hydrogen and oxygen and is

* To whom correspondence should be addressed. Tel.: +98 711 2303071. Fax: +98 711 6287294. E-mail: rahimpor@shirazu.ac.ir.

10.1021/ie9005113
Published on Web 12/03/2009

based on inorganic membranes such as Pd and ceramic membranes.[20] In many hydrogen-related reaction systems, Pd−alloy membranes on stainless steel supports have been used as hydrogen-permeable membranes.[21] The highest hydrogen permeability was observed at an alloy composition of 23 wt % silver.[22] Palladium-based membranes have been used for decades in hydrogen extraction because of their high permeability and good surface properties and because palladium, like all metals, is 100% selective for hydrogen transport.[23] These membranes combine excellent hydrogen transport and discrimination properties with resistance to high temperatures, corrosion, and solvents. Key requirements for the successful development of palladium-based membranes are low costs, as well as permselectivity combined with good mechanical/thermal and long-term stability.[24] These properties make palladium-based membranes such as Pd−Ag membranes very attractive for use with petrochemical gases. To make such membranes, a thin palladium or palladium-based alloy layer is prepared on the surface or inside the pores of a porous support. Much research has been devoted to developing supports for palladium or palladium-based alloy membranes, such as the works of Huribert et al.,[25] Pugachev et al.,[26] and Keuler et al.[27] The materials commercially used for porous supports are ceramics, stainless steel, and glass. For metallic composite membranes, the support should be porous, smooth-surfaced, highly permeable, thermally stable, and adherent to metals.[28]

1.3. Membrane Reactors. Membrane reactors have been applied to many common classes of catalytic reactions including dehydrogenation, hydrogenation, and partial and total oxidation reactions. For hydrogenation reactions involving liquid hydrocarbons, the membrane's role is to separate the liquid from the gaseous reactant (e.g., hydrogen) and to provide a means for delivering this reactant at a controlled rate. Doing the latter reportedly helps to avoid hot spots in the reactor or undesirable side reactions.[29]

The general advantages of membrane reactors as compared to sequential reaction−separation systems are (1) increased reaction rates, (2) reduced byproduct formation, (3) lower energy requirements, and (4) the possibility of heat integration.

These advantages potentially lead to compact process equipment that can be operated with a high degree of flexibility.[30]

1.4. Fluidized-Bed Reactor. Conventional Packed-Bed Reactors (PBRs) are seriously limited by poor heat transfer and low catalyst particle effectiveness factors because of severe diffusion limitations for the catalyst particle sizes used.[31] Smaller particle sizes are infeasible in packed-bed systems because of pressure drop considerations.[32] One of the main advantages of fluidized-bed reactors is the excellent tube-to-bed heat transfer, which allows for safe and efficient reactor operation even for highly exothermic reactions. Also for highly endothermic reactions, where the hot catalyst is circulated between the reactor and the regenerator, the excellent gas−solid heat-transfer characteristics of fluidized beds can be effectively exploited.[33] Membranes are incorporated to improve reactor performance,[34] and this performance is strongly dependent on the active membrane surface area.[35]

Membrane can be improved by fluidization behavior as a result of compartmentalization and reduced average bubble size due to enhanced bubble breakage, resulting in improved bubble-to-emulsion mass transfer. Some of the possible disadvantages of fluidized-bed membrane reactors are problems such as difficulties in reactor construction, membrane sealing at the wall, erosion of the reactor internals, and catalyst attrition.[33]

1.5. Objectives. In this work, we decided to study the effect of hydrogen redistribution along a fluidized-bed membrane reactor. In the first strategy, hydrogen permeation was applied so that the first segment (bottom of the second reactor) of the reactor used more hydrogen, whereas in the second strategy, the last segment (top of the second rector) of the reactor used more hydrogen. We used a dynamic two-phase theory in the bubbling regime of fluidization in order to model and compare the performance of the two methods of hydrogen redistribution. Therefore, there are two typical modes in the feed synthesis gas flow direction against the reacting gas flow in the synthesis gas-cooled reactor of the dual-type methanol reactor: cocurrent (in parallel flow) and countercurrent (in counter flow).[36−38] Comparison between the different strategies shows that the reactor in the second strategy (countercurrent configuration) operates with a higher conversion of methanol, longer catalyst life, and higher carbon dioxide removal whereas the reactor in the first strategy (cocurrent configuration) operates with a higher carbon monoxide removal, lower water production, and higher hydrogen permeation rate. The model was also validated against observed plant data for the conventional methanol reactor of the Shiraz Petrochemical Complex (Zagross Petrochemical Company of Iran).

2. Process Description

Fluidized-Bed Membrane Dual-Type Methanol Reactor (FBMDMR) in Countercurrent and Cocurrent Modes. The process of methanol synthesis in a fluidized-bed membrane dual-type reactor in countercurrent mode has been studied by Rahimpour et al.[17]

The difference between the methanol synthesis process in countercurrent and cocurrent modes is in the direction of the synthesis gas flowing through the tubes of the second reactor. In countercurrent mode, the feed synthesis gas is fed to the tubes in the opposite direction of the reacting gas from the top of the reactor, whereas in cocurrent mode, the synthesis gas flows through the tubes in the same direction as the reacting gas mixture stream in the shell side. A schematic diagram of a fluidized-bed membrane dual-type methanol reactor in countercurrent and cocurrent configurations for methanol synthesis is presented in Figure 1.

The technical design data for the catalyst pellets and the input data are similar for the cocurrent and countercurrent configurations.[17]

3. Mathematical Model

3.1. Water-Cooled Reactor (First Reactor). A heterogeneous model accounting for the gas and catalyst phases was developed to describe the reactor. The balances typically account for convection and transport to the solid phase. We considered some basic assumptions in the model as follows: (a) Axial dispersion is neglected. (b) One-dimensional flow is considered. (c) The plug-flow regime is assumed. (d) All gases are ideal. (e) Radial diffusion in catalyst pellet is neglected.

Model Structure. The mass and energy balance equations for the catalyst pellets can be formulated as

$$\frac{\partial y_i^s}{\partial t} - \frac{k_{gi} a_v}{\varepsilon_s}(y_i - y_i^s) - \frac{\rho_B \eta a r_i}{\varepsilon_s c_t} = 0 \qquad i = 1, 2, 3, ..., N-1 \tag{1}$$

$$\frac{\partial T}{\partial t} - \frac{h_f a_v}{\rho_B \varepsilon_s c_{ps}}(T - T_s) - \frac{a\eta}{\varepsilon_{ps} c_{ps}} \sum_{j=1}^{n} r_j(-\Delta H_{f,i}) = 0 \tag{2}$$

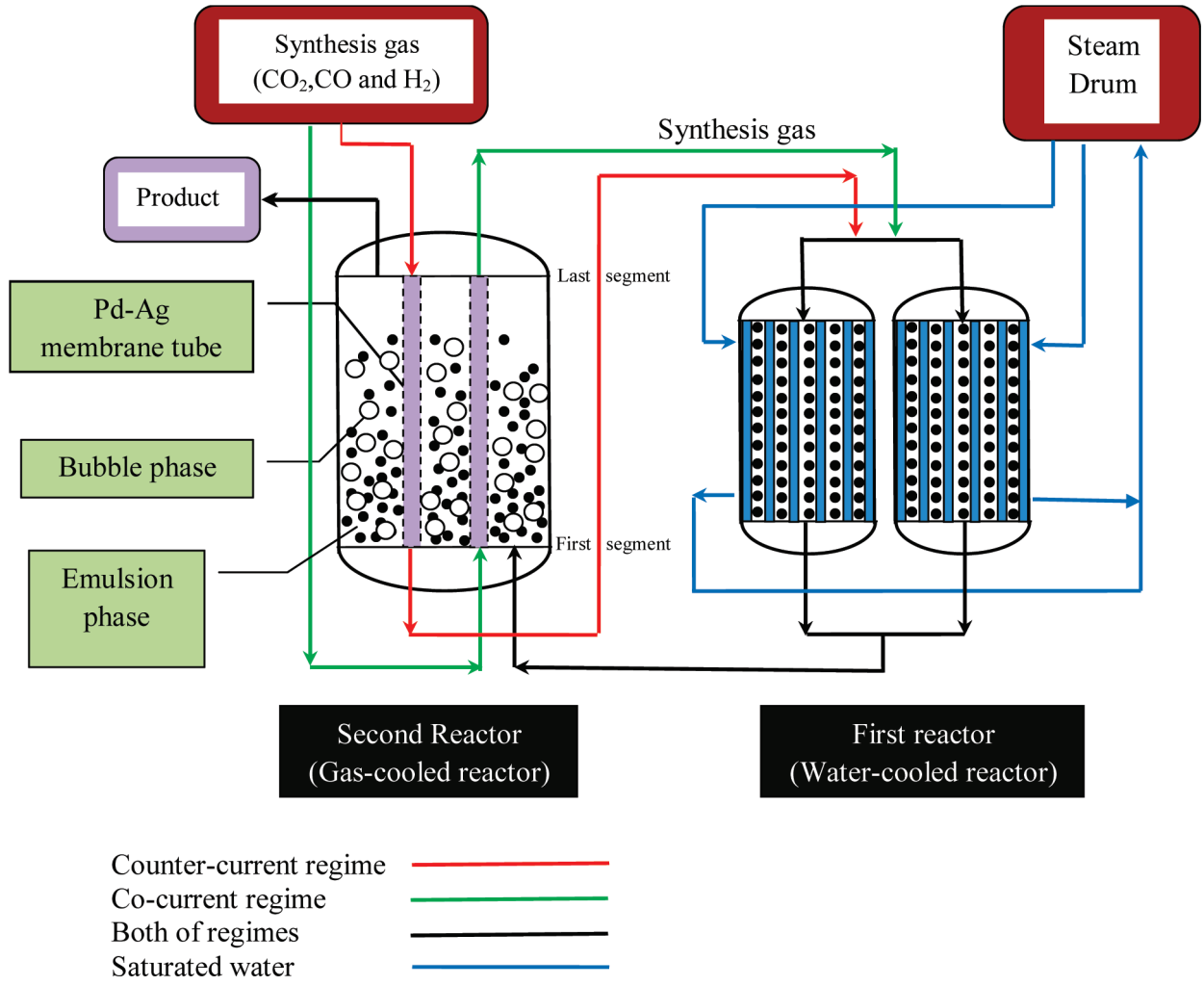

Figure 1. Schematic flow diagram of fluidized-bed membrane dual-type methanol reactor in countercurrent and cocurrent modes.

η is the effectiveness factor of catalyst and is calculated according to the procedure explained by Rezaie et al.[39] Moreover, the kinetic model and the equilibrium rate constants were selected from Graaf's studies.[40,41]

The following two conservation equations can be written for the fluid phase

$$\frac{\partial y_i}{\partial t} + \frac{F_t}{A_c \varepsilon_B c_t}\frac{\partial y_i}{\partial z} - \frac{a_v k_{gi}}{\varepsilon_B}(y_i^s - y_i) = 0 \qquad i = 1, 2, 3, ..., N-1 \quad (3)$$

$$\frac{\partial T}{\partial t} + \frac{F_t}{A_c \varepsilon_B c_t}\frac{\partial T}{\partial z} - \frac{a_v h_f}{\varepsilon_B c_t c_{pg}}(T_s - T) - \frac{\pi D_i}{A_c \varepsilon_B c_t c_{pg}} U_{shell}(T_{shell} - T) = 0 \quad (4)$$

The boundary conditions are as follows

$$z = 0 \qquad y_i = y_{i_{in}} \qquad T = T_{in} \quad (5)$$

3.2. Gas-Cooled Reactor (Second Reactor).

3.2.1. Shell Side (Reaction Side). Model Assumptions. The conservation of mass and heat in the fluidized-bed reactor (shell side) was developed on the basis of the following assumptions: (a) The gas fed to the fluidized bed through membranes is assumed to be initially perfectly mixed or extracted from the emulsion phase (because of the relatively small bubble fraction). (b) The dense catalyst bed is considered to be composed of a bubble phase and an emulsion phase. (c) The operation is assumed to be isothermal, which means that the bubble and emulsion phases have same temperature. (d) The plug-flow regime in the bubble phase is assumed. (e) The axial diffusion of hydrogen through the membrane is neglected compared to the radial diffusion. (f) The bubble rise velocity is constant and equal to the average value. (g) Ideal gas behavior is assumed. (h) The solids concentration in the freeboard is assumed to decay exponentially as proposed by Kunii and Levenspiel[42]

$$\phi = \phi^* + (\phi_d - \phi^*)\exp(-a_{freeboard} z_{freeboard}) \quad (6)$$

(i) Bubbles are assumed to be spherical with a constant size equal to the average value.

The gas in the bubble phase is in plug flow and contains some catalyst particles, which are involved in reactions, but the extent of reaction in the bubble phase is much less than that in the emulsion phase.

Model Structure. An element of length Δz as depicted in Figure 2 was considered. On the basis of the aforementioned assumptions, the bubble- and emulsion-phase mass conservation equations are formulated as

Bubble phase

$$\frac{\partial y_i^b}{\partial t} + \frac{1}{A_{shell} c_t}\frac{\partial F_i^b}{\partial z} - k_{bei} a_b (y_i^e - y_i^b) - \frac{\gamma a \rho_s}{c_t}\sum_{i=1}^{3} r_{bij} = 0 \qquad i = 1, 2, 3, ..., N-1 \quad (7)$$

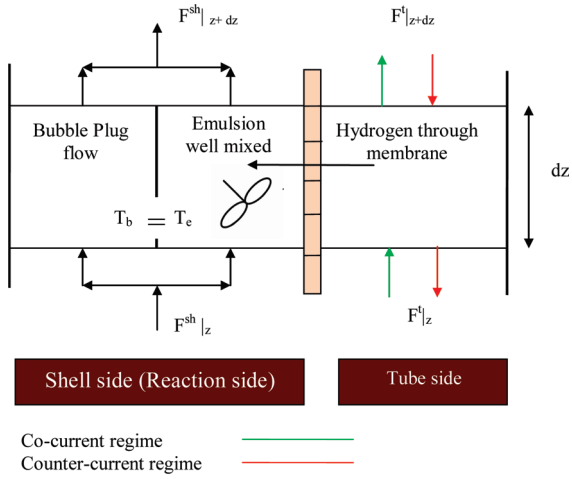

Figure 2. Schematic diagram of an elemental volume of a fluidized-bed membrane reactor in cocurrent and countercurrent modes.

Emulsion phase

$$\frac{\partial y_i^e}{\partial t} + \frac{1}{A_{shell}c_t}\frac{\partial F_i^e}{\partial z} - \frac{\rho_e a\eta}{c_t}\sum_{j=1}^{3} r_{ij} - \frac{\delta k_{bei} a_b}{(1-\delta)}(y_i^b - y_i^e) - \frac{\alpha_H}{A_s c_t}\left(\sqrt{P_H^t} - \sqrt{P_H^{sh}}\right) = 0 \quad (8)$$

F_i^b and F_i^e are given by

$$F_i^b = y_i^b F^{sh} \qquad F_i^e = y_i^e F^{sh} \quad (9)$$

The heat-transfer equation between the bed and tubes is

$$\frac{\partial T}{\partial t} + (1-\delta)\frac{\alpha_H}{A_s c_t c_{pg}}\left(\sqrt{P_H^t} - \sqrt{P_H^{sh}}\right)c_{pH}(T - T_{tube}) - \frac{(1-\delta)\eta a\rho_e}{c_t c_{pg}}\sum_{j=1}^{3} r_j(\Delta H_{fj}) + \frac{\delta\gamma a\eta}{c_t c_{pg}}\sum_{j=1}^{3} r_{bj}(-\Delta H_{fj}) - \frac{\pi D_i}{A_{shell}c_t c_{pg}}U_{shell}(T_{tube} - T) = 0 \quad (10)$$

3.2.2. Tube Side (Fresh Feed Synthesis Gas Flow). The mass and energy balance equations for the fluid phase are given by

$$\frac{\partial y_i}{\partial t} \pm \frac{F_t}{A_c c_t}\frac{\partial y_i}{\partial z} + \frac{\alpha_H}{A_s c_t}\left(\sqrt{P_H^t} - \sqrt{P_H^{sh}}\right) = 0 \qquad i = 1, 2, 3, ..., N-1 \quad (11)$$

$$\frac{\partial T_{tube}}{\partial t} \pm \frac{F^t}{A_c c_t c_{pg}}c_{pg_{tube}}\frac{\partial T_{tube}}{\partial z} + \frac{\alpha_H}{A_s c_t c_{pg}} \times \left(\sqrt{P_H^t} - \sqrt{P_H^{sh}}\right)c_{pH}(T - T_{tube}) - \frac{\pi D_i}{A_c c_t c_{pg}}U_{tube}(T - T_{tube}) = 0 \quad (12)$$

The boundary conditions are

$$z = L \qquad y_i = y_{if} \qquad T = T_f \quad (13)$$

In eqs 11 and 12, the positive sign is used for cocurrent mode, and the negative sign is for countercurrent mode.

Auxiliary correlations for the estimation of the mass- and heat-transfer coefficients and the empirical correlations for the hydrodynamic parameters in the proposed model were extracted from the published literature.[17] Also, the deactivation model for the commercial methanol synthesis catalyst $CuO/ZnO/Al_2O_3$ was adopted from Hanken's studies.[43]

Table 1. Comparison of Elnashaie et al.'s Model[16] with the Proposed FMDMR Model

composition (%)	Elnashaie et al.'s model[16]	FMDMR model	error (%)
CO	1.881	1.38	–26.6
H_2	73.512	75.38	2.54
CH_3OH	4.744	4.92	3.71
CO_2	2.838	3.12	9.93
H_2O	1.809	1.68	–7.131
N_2	2.356	2.31	–1.95
CH_4	12.86	11.21	–12.8

Table 2. Comparison between Predicted Methanol Production Rate and Plant Data

time (days)	plant capacity (tons/day)	predicted capacity (tons/day)	error (%)
0	295.0	308.8	2.93
100	296.5	297.03	0.18
200	302.6	289.1	–4.46
300	284.3	283.09	–0.44
400	277.9	278.19	–0.10
500	278.2	274.03	–1.50
600	253.0	270.41	6.88
700	274.0	267.19	–2.48
800	268.1	264.30	–1.65
900	275.5	261.67	–5.02
1000	274.6	259.25	–5.58
1100	262.9	257.02	–2.24
1200	255.2	255.18	–0.05

The permeation rate of hydrogen through the Pd−Ag membrane, j_H (mol/s), was assumed to obey the half-power pressure law (Sievert's law)

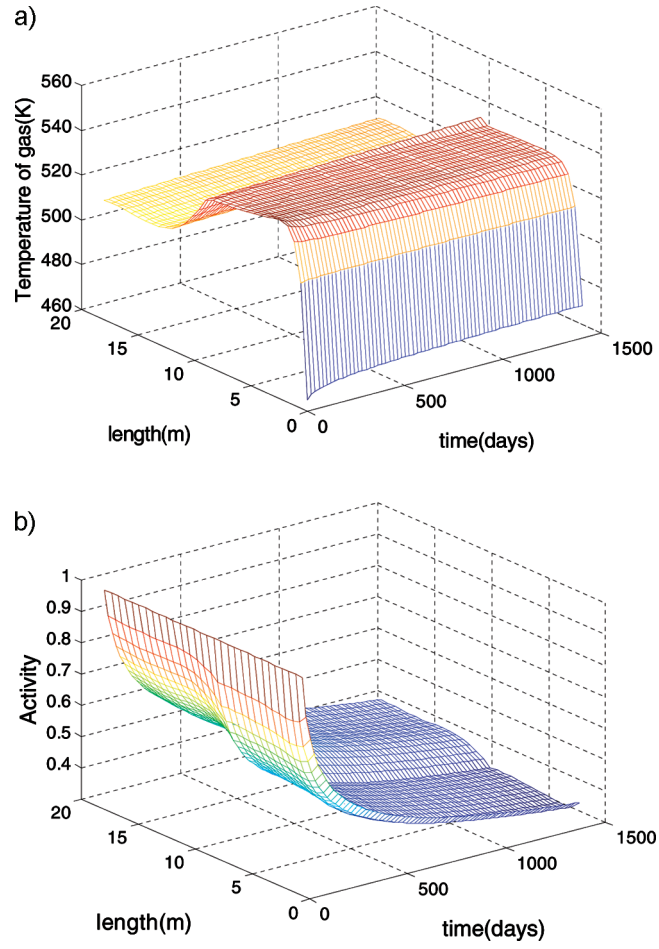

Figure 3. Profiles of (a) temperature and (b) catalyst activity versus time and length for an FMDMR in cocurrent mode.

$$j_H = \alpha_H\left(\sqrt{P_H^t} - \sqrt{P_H^{sh}}\right) \quad (14)$$

The hydrogen permeation rate constant (α_H) was calculated according to procedure explained by Hara et al.[44]

4. Numerical Solution

The governing equations of the model form a system of coupled equations comprising partial derivative equations of mass and energy conservation rules for the catalyst, fluid, bubble, and emulsion phases; the ordinary differential equation of the deactivation model; and also nonlinear algebraic equations of the kinetic model. The system of equations was solved using a two-stage approach consisting of a steady-state identification stage followed by a dynamic solution stage.

After rewriting the model equations, a set of differential algebraic equations (DAEs) is obtained for both cocurrent and countercurrent modes. This set of equations is changed to nonlinear algebraic equations (NAEs) using the backward finite-difference approximation. The NAEs constitute a boundary-value problem that was solved using the shooting method in countercurrent mode and the trial-and-error method in cocurrent mode. In this way, the initial conditions for temperature and component concentrations were determined for the dynamic simulation. The set of dynamic equations was discretized with respect to axial and time coordinates on the nodes.

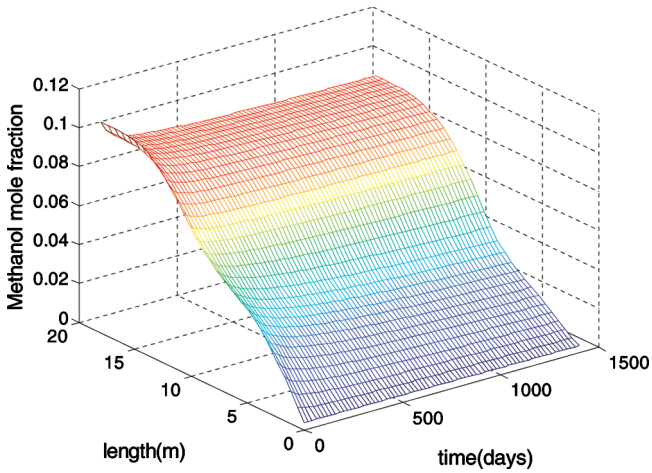

Figure 4. Profiles of mole fraction of methanol versus time and length for an FMDMR in cocurrent mode.

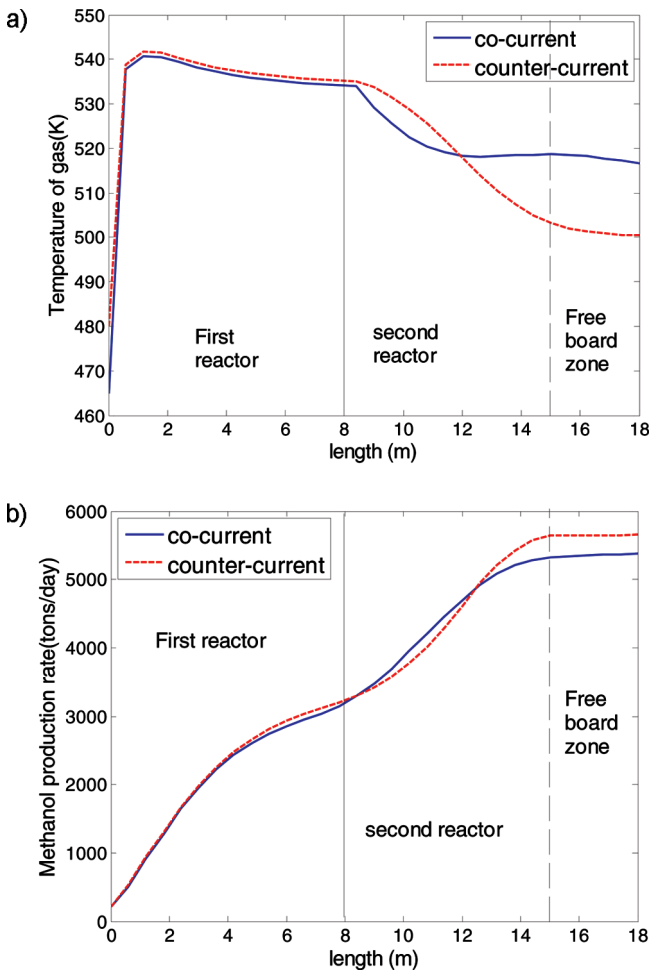

Figure 5. Profiles of (a) temperature and (b) production rate along the reactor for cocurrent and countercurrent modes for fresh catalyst.

4.1. Solution Procedure for Countercurrent Mode. In countercurrent mode, the temperature (T_{in}) and hydrogen mole fraction (y_{in}) of the inlet feed synthesis gas to the water-cooled reactor are unknown (initial conditions), whereas the temperature (T_f) and hydrogen mole fraction (y_f) of the feed synthesis gas stream are known (final condition). The shooting method converts the boundary-value problem into an initial-value problem. The solution is possible by guessing values for T_{in} and y_{in} for the heated feed synthesis gas to the water-cooled reactor. The water-cooled and gas-cooled reactors were divided into 14 and 16 sections, respectively, and then the Gauss−Newton method was used to solve the nonlinear algebraic equations in each section. At the end, the calculated values of temperature (T_f) and hydrogen mole fraction (y_f) of the fresh feed synthesis gas stream were compared with the actual values. This procedure was repeated until the specified terminal values were achieved within a small convergence criterion.

4.2. Solution Procedure for Cocurrent Mode. In cocurrent mode, the calculation was started with initial guesses for T_{in} and y_{in}, which are unknown (initial conditions). The initial conditions were calculated using the Gauss−Newton method replaced by its previous value in subsequent calculations. Substitution was continued until the convergence criterion was met.

The globally convergent multidimensional Newton's method in the Matlab programming environment was used to solve these equations.

5. Results and Discussion

5.1. Model Validation. The validation of the steady-state and dynamic model for the industrial dual-type methanol reactor with plant data was previously performed by Rahimpour et al.[10] It was observed that the model performed satisfactorily under industrial conditions, giving good agreement between the daily observed plant data and the simulation data.[10,13]

5.1.1. Steady-State Model Validation. As stated before, Elnashaie et al.[16] mathematically studied a fluidized-bed configuration for methanol synthesis and presented a steady-state model based on the two-phase theory of fluidization. The results of Elnashaie et al.'s model[16] were compared with those of our suggested steady-state model in Table 1 to check the simulation of the fluidized-bed membrane dual-type reactor. Evidently, our numerical predictions are in good qualitative agreement with Elnashaie et al.'s model.

5.1.2. Dynamic Model Validation. To verify the "goodness" of the dynamic model, simulation results were compared with the historical process data of a single-type reactor. The predicted results for the production rate and the corresponding observed

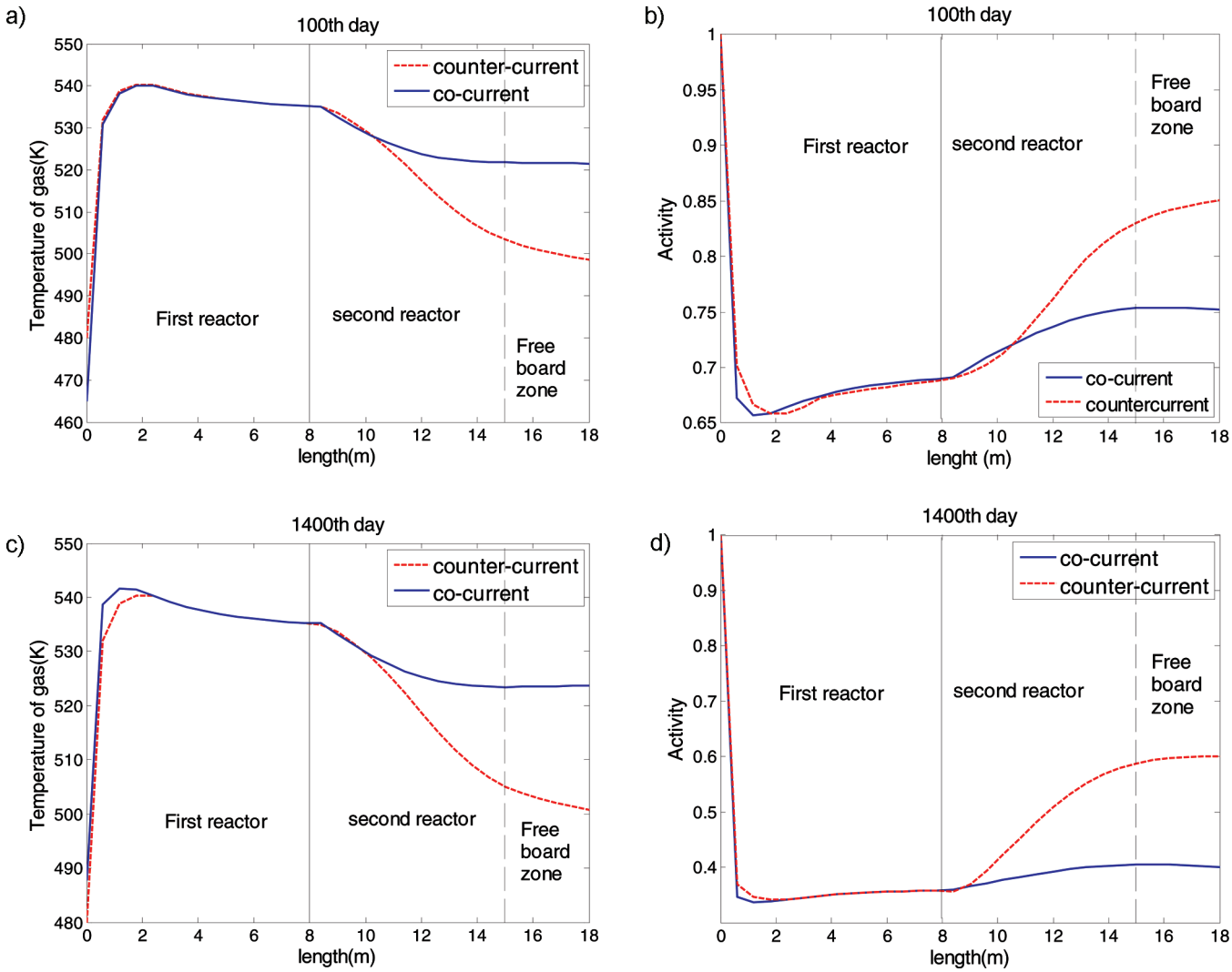

Figure 6. Profiles of temperature and activity along the reactor for cocurrent and countercurrent modes at the (a,b) 100th and (c,d) 1400th days of operation.

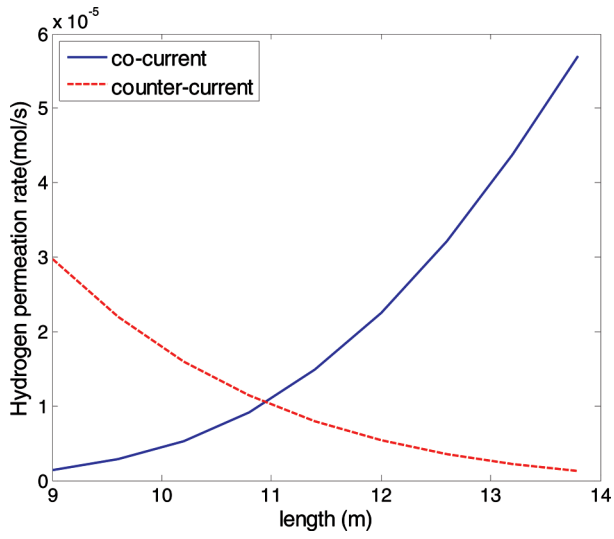

Figure 7. Permeation rate of hydrogen along the reactor for cocurrent and countercurrent modes for fresh catalyst.

data of the plant are presented in Table 2. It was observed that the model performed satisfactorily under the industrial conditions and that the daily observed plant data were in good agreement with the simulation data.

A parametric analysis was performed to address the vital issues, such as temperature, catalyst activity, methanol mole fraction, and methanol production rate profiles, along the reactors. Figure 3a,b illustrates the profiles of the reactor temperature and catalyst activity versus time and length for a fluidized-bed membrane dual-type methanol reactor in cocurrent mode. In the first reactor (from the reactor entrance to 8 m), the temperature of the reacting gas mixture in the first days is higher because of the fresh catalyst and higher conversion. The rate of reaction heat decreases during further operation as the catalyst is deactivated. Because the reaction heat is continuously removed by the water coolant, the temperature of the reacting gas mixture is reduced with time in the first reactor. In the second reactor (from 8 to 18 m), catalyst deactivation leads to an increase in the methanol concentration gradient along the reactor, and therefore, the reaction heat rises with time. Because the ability of the coolant gas to remove reaction heat is less than that of the coolant water, the temperature along the second reactor decreases with time, as shown in Figure 3a. The minimum activity level is observed near the first reactor inlet, which is exposed to higher temperatures at a different time. The catalyst in the gas-cooled reactor tends to have a lower temperature, which improves the catalyst activity in this reactor, as shown in Figure 3b. Also, this figure shows that, during the operating time, the catalyst is deactivated as a result of poisoning

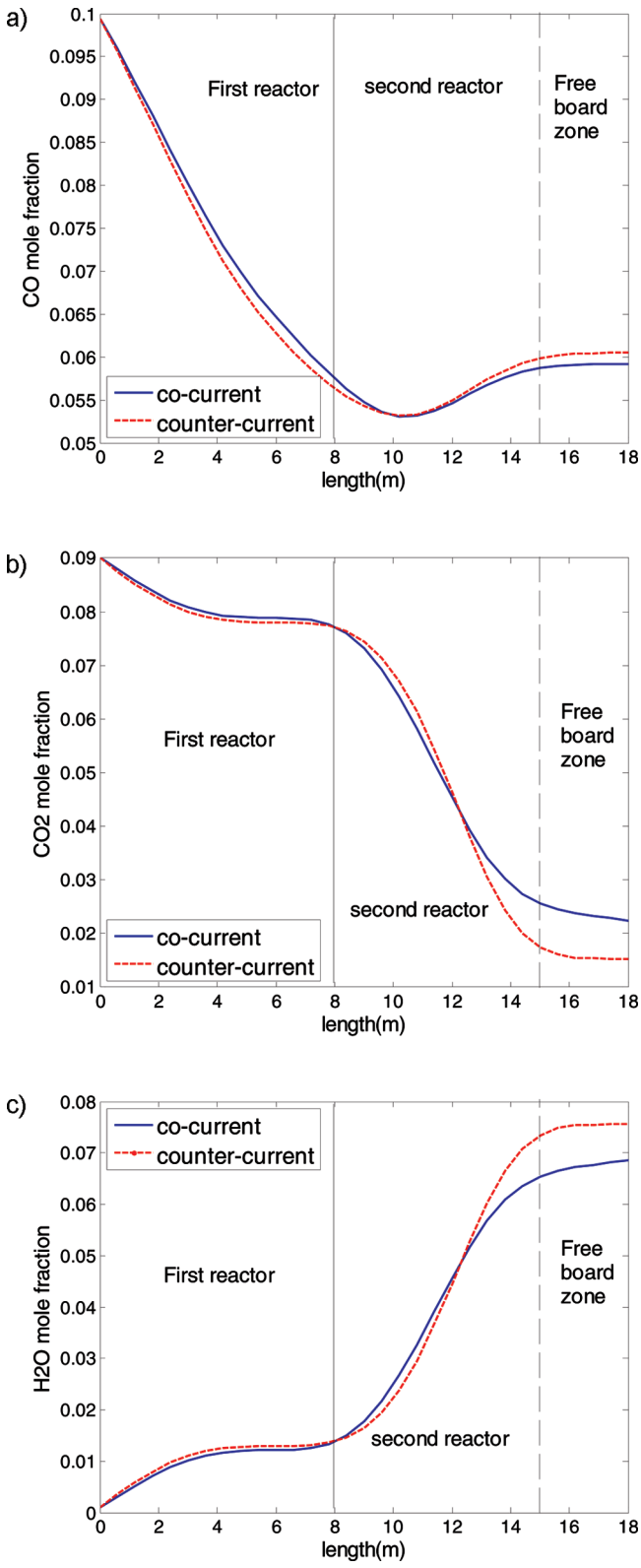

Figure 8. Comparison between CO, CO_2, and H_2O mole fractions in cocurrent and countercurrent modes.

and thermal sintering, which is the loss of catalyst active surface area owing to crystallite growth of either the support material or the active phase.

Figure 4 shows the methanol mole fraction profiles versus time and length for a fluidized-bed membrane dual-type methanol reactor in cocurrent mode. As can be seen, the mole fraction of methanol increases along the reactor, whereas it decreases with time as a result of catalyst deactivation.

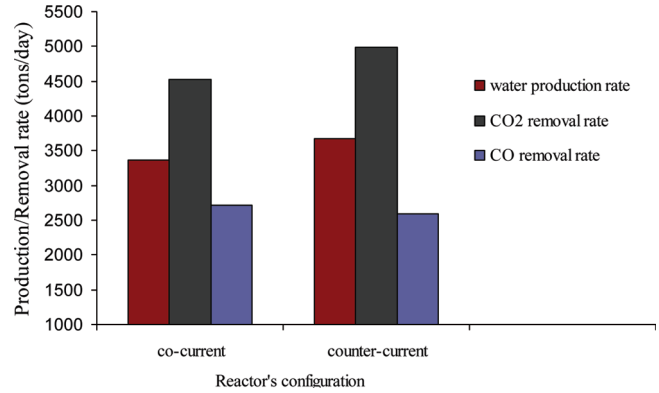

Figure 9. Comparison water production rate and CO_2 and CO removal rates in cocurrent and countercurrent modes on the first day.

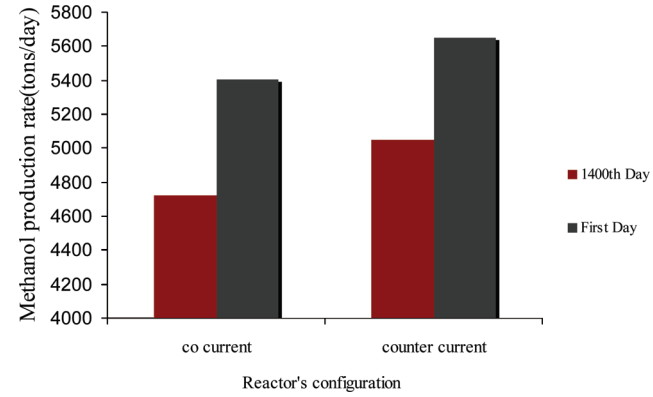

Figure 10. Comparison of methanol production in cocurrent and countercurrent modes on the first and 1400th days.

5.2. Comparison of Cocurrent and Countercurrent Modes in a Fluidized-Bed Membrane Dual-Type Methanol Reactor. Figure 5 shows a comparison between the temperature profiles and the production rate profiles along the cocurrent and countercurrent reactor configurations. As can be seen in Figure 5a, the first reactor operates at higher temperature in countercurrent configuration with respect to cocurrent configuration because the feed synthesis gas to the first reactor is preheated more in the countercurrent configuration along the second reactor. Because the reactions in the first reactor are kinetics-limited, the higher temperature in the countercurrent configuration in the first reactor enhances the reaction, and the production rate is higher than in the cocurrent configuration, as shown in Figure 5b.

The net result of Figure 5 is that the reactor can operate at suitable temperature in countercurrent mode along the reactor.

Comparisons between the temperature and activity profiles along the reactor for both types of flow at the 100th and 1400th days of operation are presented in Figure 6. As seen from Figure 6a,c, the results are similar for the temperature profiles in cocurrent and countercurrent modes at any time of operation. Therefore, the lower temperature in countercurrent mode improves the catalyst activity, which results in more efficient use of the catalyst.

Figure 7 illustrates the hydrogen permeation rate along the reactor for fresh catalyst in cocurrent and countercurrent modes. The results show that the hydrogen permeation rate in cocurrent mode is higher than that in countercurrent mode. Even though the hydrogen partial pressure difference in the last segment of the second reactor for countercurrent mode is higher than that for cocurrent mode, the effect of increasing the temperature

overcomes the effect of the hydrogen partial pressure difference, so the permeation rate of hydrogen in cocurrent mode is higher.

Figure 8a−d shows comparisons between the carbon monoxide, carbon dioxide, and water mole fractions in cocurrent and countercurrent modes for fresh catalyst. The simulation results indicate that the carbon monoxide and water mole fractions in cocurrent mode are lower than those in countercurrent mode, but the carbon dioxide mole fraction in countercurrent mode is higher. Consequently, countercurrent mode is suitable from the point of view of carbon dioxide removal, whereas the reactor in cocurrent configuration operates with higher carbon monoxide removal and lower water production.

Comparisons between the water production rate and the carbon dioxide and carbon monoxide removal rates along cocurrent and countercurrent reactor configurations for fresh catalyst are illustrated in Figure 9.

A comparison of the methanol production rate in the two different configurations of the reactor on the 1st day and 1400th day is presented in Figure 10. As can be seen, there is a considerable increase in tmethe hanol production rate in countercurrent mode at both times.

6. Conclusions

In this article, two different hydrogen redistribution strategies along a bubbling fluidized-bed membrane hydrogen permselective reactor have been compared. In the first strategy, hydrogen permeation (cocurrent configuration) is such that the first segment of the reactor uses more hydrogen, whereas in the second strategy (countercurrent configuration), the last segment of the reactor uses more hydrogen. A dynamic two-phase theory in the bubbling regime of fluidization to model and compare the performance the two methods of hydrogen redistribution was developed. Comparison between the cocurrent and countercurrent modes of operation shows that the reactor in countercurrent configuration operates with a higher conversion of methanol, longer catalyst life, and higher carbon dioxide removal, whereas the reactor in cocurrent configuration operates with a higher carbon monoxide removal, lower water production, and higher hydrogen permeation rate.

Acknowledgment

The authors thank Zagross Petrochemical Company of Iran for providing valuable operating data.

Nomenclature

a = activity
A_c = cross-sectional area of each tube (m^2)
$a_{freeboard}$ = freeboard decay constant (m^{-1})
A_i = inner area of each tube (m^2)
A_o = outside area of each tube (m^2)
A_s = lateral area of each tube (m^2)
A_{shell} = cross-sectional area of shell (m^2)
a_v = specific surface area of catalyst pellet ($m^2\ m^{-3}$)
c_{pg} = specific heat of the gas at constant pressure (J $mol^{-1}\ K^{-1}$)
c_{pH} = specific heat of the hydrogen at constant pressure (J $mol^{-1}\ K^{-1}$)
c_{ps} = specific heat of the catalyst at constant pressure (J $mol^{-1}\ K^{-1}$)
c_t = total concentration (mol m^{-3})
D = reactor diameter (m)
F_i^b = molar flow of component i in the bubble side (mol s^{-1})
F_i^e = molar flow of component i in the emulsion side (mol s^{-1})
F^{sh} = total molar flow in the shell side (mol s^{-1})
F_t = total molar flow per tube (mol s^{-1})
h_f = gas−solid heat transfer coefficient (W $m^{-2}\ K^{-1}$)
j_H = permeation rate of hydrogen through the Pd−Ag membrane (mol/s)
K_{bei} = mass-transfer coefficient for component i in the fluidized bed (m s^{-1})
k_{gi} = mass-transfer coefficient for component i (m s^{-1})
P = total pressure (Pa)
P_H^t = tube-side pressure (Pa)
P_H^{sh} = shell-side pressure (Pa)
r_{bi} = reaction rate of component i in bubble phase (mol $kg^{-1}\ s^{-1}$)
r_i = reaction rate of component i (mol $kg^{-1}\ s^{-1}$)
t = time (s)
T = bulk gas-phase temperature
T_f = final temperature of the feed synthesis gas stream (K)
T_{in} = inlet temperature of the inlet feed synthesis gas (K)
T_s = temperature of the solid phase (K)
T_{shell} = temperature of the coolant stream, in the first reactor (K)
T_{tube} = temperature of the coolant stream, in the second reactor (K)
U_{shell} = overall heat-transfer coefficient between the coolant and process streams (W $m^{-2}\ K^{-1}$)
y_i = mole fraction of component i in the fluid phase
y_i^b = mole fraction of component i in the bubble phase
y_i^e = mole fraction of component i in the emulsion phase
y_i^s = mole fraction of component i in the solid phase
z = axial reactor coordinate (m)
$z_{freeboard}$ = axial coordinate in the freeboard zone (m)

Greek Letters

α_H = hydrogen permeation rate constant (mol $m^{-1}\ s^{-1}\ Pa^{-0.5}$)
$\Delta H_{f,i}$ = enthalpy of formation of component i (J mol^{-1})
ε_B = void fraction of the catalytic bed
ε_s = void fraction of the catalyst
ν = stoichiometric coefficient
ρ = density of fluid phase
ρ_B = density of the catalytic bed (kg m^{-3})
ρ_s = density of the catalyst (kg m^{-3})
η = catalyst effectiveness factor
δ = bubble-phase volume as a fraction of total bed volume
ϕ = solids volume fraction
ϕ^* = saturation carrying capacity
ϕ_d = solids volume fraction in the dense phase

Superscripts and Subscripts

b = bubble phase
e = emulsion phase
f = feed conditions
i = component i
sh = shell side
t = tube side

Abbreviations

FBMDMR = fluidized-bed membrane dual-type methanol reactor
IDMR = industrial dual-type methanol reactor

Literature Cited

(1) *Methanol Basics*; Technical Report EPA 400-F-92-009; U.S. Environmental Protection Agency: Washington, DC, 1994. Available at http://www.epa.gov/otaq/consumer/07-meoh.pdf (accessed Apr 2005).

(2) *Clean Alternative Fuels: Methanol*; Technical Report EPA 420-F-00-040; U.S. Environmental Protection Agency: Washington, DC, 2002. Available at http://www.naftc.wvu.edu/NAFTC/data/factsheets/methfactsheetepa.pdf (accessed Jul 2005).

(3) Gallucci, F.; Basile, A.; Drioli, E. Methanol as an Energy Source and/or Energy Carrier in Membrane Processes. *Sep. Purif. Rev.* **2007**, *36* (2), 175.

(4) Highfield, J. G.; Bill, A.; Eliasson, B.; Geiger, F.; Uenala, E. The Role of Simple Alcohols in Renewable Hydrogen Energy Cycles. Presented at the 11th International Symposium on Alcohol Fuels Technology (ISAF XI), Sun City, South Africa, Apr 14−17, 1996.

(5) Demirbas, A. Biodiesel Production from Vegetable Oils by Supercritical Methanol. *J. Sci. Ind. Res.* **2005**, *64*, 858.

(6) Lovik, I.; Hillestad, M.; Hertzberg, T. Long Term Dynamic Optimization of a Catalytic Reactor System. *Comput. Chem. Eng.* **1998**, *22*, 707.

(7) Rahimpour, M. R.; Fathikalajahi, J.; Jahanmiri, A. Selective Kinetic Deactivation Model for Methanol Synthesis from Simultaneous Reaction of CO_2 and CO with H_2 on a Commercial Copper/Zinc Oxide Catalyst. *Can. J. Chem. Eng.* **1998**, *76*, 753.

(8) Velardi, S. A.; Barresi, A. A. Methanol Synthesis in a Forced Unsteady-State Reactor Network. *Chem. Eng. Sci.* **2002**, *57* (15), 2995.

(9) Rahimpour, M. R. A Two-Stage Catalyst Bed Concept for Conversion of Carbon Dioxide into Methanol. *Fuel Process. Technol.* **2008**, *89* (5), 556.

(10) Rahimpour, M. R.; Lotfinejad, M. A Comparison of Co-current and Counter-current Modes of Operation for a Dual-type Industrial Methanol Reactor. *Chem. Eng. Process.* **2008**, *47*, 1819.

(11) Rahimpour, M. R.; Khosravanipour Mostafazadeh, A.; Barmaki, M. M. Application of Hydrogen-Permselective Pd-based Membrane in an Industrial Single-type Methanol Reactor in the Presence of Catalyst Deactivation. *Fuel. Process. Technol* **2008**, *89* (12), 1396.

(12) Rahimpour, M. R.; Ghader, S. Enhancement of CO Conversion in a Novel Pd−Ag Membrane Reactor for Methanol Synthesis. *Chem. Eng. Process.* **2004**, *43*, 1181.

(13) Rahimpour, M. R.; Lotfinejad, M. Enhancement of Methanol Production in a Membrane Dual-type Reactor. *Chem. Eng. Technol.* **2007**, *30*, 1062.

(14) Rahimpour, M. R.; Lotfinejad, M. Co-current and Counter-current Configurations for a Membrane Dual-type Methanol Reactor. *Chem. Eng. Technol.* **2008**, *31* (1), 38.

(15) Rahimpour, M. R.; Alizadehhesari, K. Enhancement of Carbon Dioxide Removal in a Hydrogen-Permselective Methanol Synthesis Reactor. *Int. J. Hydrogen Energy* **2009**, *34* (3), 1349.

(16) Wagialla, K. M.; Elnashaie, S. S. E. H. Fluidized-Bed Reactor for Methanol Synthesis. A Theoretical Investigation. *Ind. Eng. Chem. Res.* **1991**, *30*, 2298.

(17) Rahimpour, M. R.; Alizadehhesari, K. A Novel Fluidized Bed Membrane Dual-type Reactor Concept for Methanol Synthesis. *Chem. Eng. Technol.* **2008**, *3* (12), 1775.

(18) Rahimpour, M. R.; Elekaei, H. Enhancement of Methanol Production in a Novel Fluidized Bed Hydrogen-permselective Membrane Reactor in the Presence of Catalyst Deactivation. *Int. J. Hydrogen Energy* **2009**, *34* (5), 2208.

(19) *Domestic Industrial Dual Type Methanol Reactor*; Design Manual; Iran, 2007.

(20) Chen, G.; Yuan, Q. Methanol Synthesis from CO_2 Using a Silicone Rubber/Ceramic Composite Membrane Reactor. *Sep. Purif. Technol.* **2004**, *34*, 227.

(21) Lin, Y.-M.; Rei, M.-H. Study on the Hydrogen Production from Methanol Steam Reforming in Supported Palladium Membrane Reactor. *Catal. Today* **2001**, *67*, 77.

(22) Rahimpour, M. R.; Ghader, S. Theoretical Investigation of a Pd-Membrane Reactor for Methanol Synthesis. *Chem. Eng. Technol.* **2003**, *26* (8), 902.

(23) Buxbaum, R. E.; Kinney, A. B. Hydrogen Transport through Tubular Membranes of Palladium Coated Tantalum and Niobium. *Ind. Eng. Chem. Res.* **1996**, *35*, 530.

(24) Dittmeyer, R.; Hollein, V.; Daub, K. Membrane Reactors for Hydrogenation and Dehydrogenation Processes Based on Supported Palladium. *J. Mol. Catal. A: Chem.* **2001**, *173*, 135.

(25) Huribert, R. C.; Konecny, J. O. Diffusion of Hydrogen though Palladium. *J. Chem. Phys.* **1960**, *43*, 655.

(26) Pugachev, V. A.; Busol, F. I.; Nikolaev, E. I.; Nam, B. P. Permeability and Diffusion of Hydrogen in Palladium−Silver Alloys. *J. Phys. Chem.* **1975**, *49*, 1781.

(27) Keuler, J. N.; Lorenzen, L. Developing a Heating Procedure to Optimize Hydrogen Permeance through Pd−Ag Membranes of Thickness Less than 2.2 μm. *J. Membr. Sci.* **2002**, *195*, 203.

(28) Ryi, S.-K.; Park, J.-S.; Kim, S.-H.; Cho, S.-H.; Park, J.-S.; Kim, D.-W. Development of a New Porous Metal Support of Metallic Dense Membrane for Hydrogen Separation. *J. Membr. Sci.* **2006**, *279*, 439.

(29) Marcano, J. G. S.; Tsotsis, T. T. *Catalytic Membranes and Membrane Reactors*; Wiley-VCH Verlag GmbH: Weinheim, Germany, 2002.

(30) Nunes, S. P.; Peinemann, K. V. *Membrane Technology in the Chemical Industry.* Wiley-VCH Verlag GmbH: Weinheim, Germany, 2001.

(31) Adris, A. M.; Elnashaie, S. S. E. H.; Hughes, R. A Fluidized Bed Membrane Reactor for the Steam Reforming of Methane. *Can. J. Chem. Eng.* **1991**, *69*, 1061.

(32) Santos, A.; Mene'ndez, M.; Santamaria, J. Partial oxidation of methane to carbon monoxide and hydrogen in a fluidized bed reactor. *Catal. Today* **1994**, *21*, 481.

(33) Deshmukh, S. A. R. K.; Heinrich, S.; Mörl, L.; van Sint Annaland, M.; Kuipers, J. A. M. Membrane Assisted Fluidized-bed Reactors: Potentials and Hurdles. *Chem. Eng. Sci.* **2007**, *62*, 416.

(34) Mahecha-Botero, A.; Chen, Z.; Grace, J. R.; Elnashaie, S. S. E. H.; Lim, C. J.; Rakib, M.; Yasuda, I.; Shirasaki, Y. Comparison of Fluidized-bed Flow Regimes for Steam Methane Reforming in Membrane Reactors: A Simulation Study. *Chem. Eng. Sci.* **2009**, *64* (16), 3598.

(35) Mahecha-Botero, A.; Boyd, T.; Gulamhusein, A.; Comyn, N.; Lim, C. J.; Grace, J. R.; Shirasaki, Y.; Yasuda, I. Pure Hydrogen Generation in a Fluidized-bed Membrane Reactor: Experimental Findings. *Chem. Eng. Sci.* **2008**, *63*, 2752.

(36) Gallucci, F.; Basile, A. Co-current and Counter-current Modes for Methanol Steam Reforming Membrane Reactor. *Int. J. Hydrogen Energy.* **2006**, *31* (15), 2243.

(37) Basile, N.; Paturzo, L.; Gallucci, F. Co-current and Counter-current Modes for Water Gas Shift Membrane Reactor. *Inst. Membr. Technol.* **2003**, *82*, 275.

(38) Thunman, H.; Leckner, B. Co-current and Counter-current Fixed Bed Combustion of Biofuel−A Comparison. *Fuel* **2003**, *82*, 275.

(39) Rezaie, N.; Jahanmiri, A.; Moghtaderi, B.; Rahimpour, M. R. A comparison of homogeneous and heterogeneous dynamic models for industrial methanol reactors in the presence of catalyst deactivation. *Chem. Eng. Process.* **2005**, *44* (8), 911.

(40) Graaf, G. H.; Scholtens, H.; Stamhuis, E. J.; Beenackers, A. A. C. M. Intra-Particle Diffusion Limitations in Low-pressure Methanol Synthesis. *Chem. Eng. Sci.* **1990**, *45* (4), 773.

(41) Graaf, G. H.; Sijtsema, P. J. J. M.; Stamhuis, E. J.; Joosten, G. E. H. Chemical Equilibrium in Methanol Synthesis. *Chem. Eng. Sci.* **1986**, *41* (11), 2883.

(42) Kunii, D.; Levenspiel, O. *Fluidization Engineering*; Wiley: New York, 1991.

(43) Hanken, L. Optimization of Methanol Reactor. Master's Thesis, Norwegian University of Science and Technology, Trondheim, Norway, 1995.

(44) Hara, S.; Xu, W. C.; Sakaki, K.; Itoh, N. Kinetics and Hydrogen Removal Effect for Methanol Decomposition. *Ind. Eng. Chem. Res.* **1999**, *38*, 488.

Received for review March 30, 2009
Revised manuscript received November 7, 2009
Accepted November 20, 2009

IE9005113